Detection of Hydrogen Peroxide Produced during the Oxygen Reduction Reaction at Self-Assembled Thiol-Porphyrin Monolayers on Gold using SECM and Nanoelectrodes

ARTICLE *in* LANGMUIR · AUGUST 2010

Impact Factor: 4.46 · DOI: 10.1021/la100444n · Source: PubMed

5 AUTHORS, INCLUDING:

Renaud Cornut
Atomic Energy and Alternative Energies Com…
25 PUBLICATIONS **372** CITATIONS
SEE PROFILE

Mario Morin
Université du Québec à Montréal
52 PUBLICATIONS **1,630** CITATIONS
SEE PROFILE

Langmuir
Article
pubs.acs.org/Langmuir

Detection of Hydrogen Peroxide Produced during the Oxygen Reduction Reaction at Self-Assembled Thiol−Porphyrin Monolayers on Gold using SECM and Nanoelectrodes

Mohamed A. Mezour, Renaud Cornut, Emad Mohamed Hussien, Mario Morin, and Janine Mauzeroll*

Laboratory for Electrochemical Reactive Imaging and Detection for Biological Systems, Department of Chemistry, NanoQAM Research Centre, Université du Québec à Montréal, C.P. 8888, Succ. Centre-ville, Montréal, QC, Canada H3C 3P8.

Received January 29, 2010. Revised Manuscript Received June 4, 2010

Porphyrin molecules were immobilized on polycrystalline gold and glassy carbon by coordinating cobalt(II) 5,10,15,20-tetraphenyl-21*H*,23*H*-porphine to a 4-aminothiophenol self-assembled monolayer. The resulting electrocatalytic activity of the metalloporphyrin-modified substrates with regard to the oxygen reduction reaction was characterized by means of cyclic voltammetry and scanning electrochemical microscopy (SECM) using nanoelectrodes of well-defined geometry. From substrate generation tip collection (SG-TC) mode SECM measurements performed under steady-state conditions and at different applied substrate potentials, it is possible to extract kinetic information relevant to electrocatalyst substrates such as metalloporphyrin-modified gold and glassy-carbon electrodes. Such an approach allows for the isolation of the unique contribution of the electrocatalyst to the oxygen reduction reaction and peroxide formation.

Introduction

Metalloporphyrins are k^4-*N*,*N*,*N*,*N* transition-metal complexes that are known to catalyze several redox reactions including the oxygen reduction reaction (ORR). In such N_4 chelates, molecular oxygen binds reversibly to the central metal ion and is reduced through at least one two-electron transfer. There have been continuous efforts toward the preparation of solid films of porphyrins because of their use as models for electron transfer and electrocatalysis reactions.[1−3] Langmuir−Blodgett,[4,5] dip-coating,[6] spin-coating,[7] electropolymerization,[8] thermoevaporation,[9] electrodeposition,[10] and self-assembled monolayers (SAMs)[11] are examples of the many techniques used to fabricate porphyrin films on solid substrates. Among them, the self-assembled monolayer approach has a competitive advantage because it yields ultrathin solid films with well-controlled structures and superior thermal and mechanical stability.[5]

To immobilize porphyrin molecules on a surface, a 4-aminothiophenol (4-ATP) SAM on a solid support was formed, followed by axial coordination of the aromatic amino group to the cobalt(II) 5,10,15,20-tetraphenyl-21*H*,23*H*-porphine. Such surface modification has been attempted on both glassy carbon and gold macroelectrodes. The use of glassy carbon as a solid support surface is not as frequently used because the exact attachment mechanism to the carbon surface remains ill-defined and this method generally produces films with large heterogeneities.[12−14] On the contrary, gold substrates are commonly used and STM experiments have provided direct evidence that a complete monolayer of 4-ATP on Au can be formed.[15] The complete self-assembly process produces a stable, highly ordered conducting film where the porphyrins are parallel to the gold surface.[11] The porphyrin is generally oriented parallel to the surface because of the densely packed 4-ATP monolayer onto which the CoTPP is adsorbed.[11] Furthermore, a concentration of 4.86×10^{-11} mol cm^{-2} for CoTPP fixed on self-assembled 4-mercaptopyridine on gold was obtained.[16] It was also shown that the reduction of O_2 by this catalyst involves a two-electron mechanism and that hydrogen peroxide is produced.[10,17,18]

Even in well-ordered systems such as SAMs, surface heterogeneities may lead to a local variation of surface coverage. For that reason, conventional electrochemical measurements based on the measure of substrate current may not uniquely isolate the contribution of the attached-to-substrate species. In this context, scanning electrochemical microscopy (SECM) is an interesting

*Corresponding author. Phone: 514-987-3000 ext. 0895. Fax: 514-987-4054. E-mail: mauzeroll.janine@uqam.ca.

(1) Zak, J.; Yuan, H.; Ho, M.; Woo, L. K.; Porter, M. D. *Langmuir* **1993**, *9*, 2772–2774.
(2) Hutchison, J. E.; Postlethwaite, T. A.; Chen, C.-h.; Hathcock, K. W.; Ingram, R. S.; Ou, W.; Linton, R. W.; Murray, R. W.; Tyvoll, D. A.; Chng, L. L.; Collman, J. P. *Langmuir* **1997**, *13*, 2143–2148.
(3) Uosaki, K.; Kondo, T.; Zhang, X.-Q.; Yanagida, M. *J. Am. Chem. Soc.* **1997**, *119*, 8367–8368.
(4) Petty, M. C. *Langmuir-Blodgett Films.*; Roberts, G. G., Ed.; Plenum Press: New York, 1990.
(5) Ulman, A. *An Introduction to Ultrathin Organic Films: From Langmuir-Blodgett Films to Self-Assembly*; Academic Press: San Diego, CA, 1991.
(6) Araki, K.; Wagner, M. J.; Wrighton, M. S. *Langmuir* **1996**, *12*, 5393–5398.
(7) Kampas, F. J.; Yamashita, K.; Fajer, J. *Nature* **1980**, *284*, 40–44.
(8) Curran, D.; Grimshaw, J.; Perera, S. D. *Chem. Soc. Rev.* **1991**, *20*, 391–404.
(9) Manivannan, A.; Nagahara, L. A.; Hashimoto, K.; Fujishima, A.; Yanagi, H.; Kouzeki, T.; Ashida, M. *Langmuir* **1993**, *9*, 771–775.
(10) Okunola, A. O.; Nagaiah, T. C.; Chen, X.; Eckhard, K.; Schuhmann, W.; Bron, M. *Electrochim. Acta* **2009**, *54*, 4971–4978.
(11) Zhang, Z.; Hou, S.; Zhu, Z.; Liu, Z. *Langmuir* **1999**, *16*, 537–540.
(12) Médard, C.; Morin, M. *J. Electroanal. Chem.* **2009**, *632*, 120–126.
(13) Bashkova, S.; Bagreev, A.; Bandosz, T. J. *Langmuir* **2003**, *19*, 6115–6121.
(14) Bashkova, S.; Bagreev, A.; Bandosz, T. J. *Ind. Eng. Chem. Res.* **2002**, *41*, 4346–4352.
(15) Rosink, J. J. W. M.; Blauw, M. A.; Geerligs, L. J.; van der Drift, E.; Rousseeuw, B. A. C.; Radelaar, S.; Sloof, W. G.; Fakkeldij, E. J. M. *Langmuir* **2000**, *16*, 4547–4553.
(16) Lu, X.; Lv, B.; Xue, Z.; Li, M.; Zhang, L.; Kang, J. *Thin Solid Films* **2005**, *488*, 230–235.
(17) Mohammad Mazloum, A.; Parvaneh, R.; Hossein, D.; Payam Ebrahimi, K.; Hamid Reza, Z.; Somayeh, K. *Electroanalysis* **2007**, *19*, 2258–2263.
(18) Chung, T. D.; Anson, F. C. *J. Electroanal. Chem.* **2001**, *508*, 115–122.

option because it allows a local characterization of substrate reactivity. SECM is being used in an increasing number of applications for the study of different electrocatalytic processes such as ORR, methanol interference during ORR, and oxygen evolution.[19] In particular, SECM has been used to study H_2O_2 production during ORR. H_2O_2 formation during ORR is generally undesirable because it lowers the efficiency of the material and can lead to electrocatalyst corrosion. As such, the preferred reaction for practical application is the direct reduction of oxygen to water. However, this involves four electrons, four protons, and molecular oxygen bond cleavage and is thus unlikely to proceed in a single elementary step. H_2O_2 is therefore consistently present in low-pH ORR either as a reaction byproduct or as an intermediate, depending on the electrocatalytic material employed. In the literature, the H_2O_2 generation from electrocatalysts has been studied locally using different SECM approaches. In many enzymatic studies, H_2O_2 detection using SECM was done in SG-TC as reported by Horrocks et al,[20] Wittstock et al.,[21,22] and Denuault et al.[23]

In the steady-state SG-TC method, the substrate material was a microelectrode undergoing ORR and the tip detected H_2O_2 by its oxidation.[19] In later studies, the same method was extended to quantify H_2O_2 generation during ORR in acidic solution for several different electrocatalysts. Another useful approach, developed by the Wittstock group,[24] relied on a transient SG-TC mode of SECM to detect H_2O_2 during ORR at macroscopic electrodes. Importantly, this study was successful in evaluating the kinetics constants of the underlying catalyst spot by comparing the oxidation current at a microelectrode obtained through a pulse sequence experiment, at short electrolysis times, to the H_2O_2 concentration profiles calculated from an analytical expression.

The redox competition mode of scanning electrochemical microscopy (RC-SECM) was used to visualize the local electrocatalytic activity of metalloporphyrin spots toward ORR.[10] This approach was developed[25] in order to overcome a significant drawback of the tip-generation substrate collection (TG-SC) SECM mode whereby the background current observed at large substrate distances prevented the acquisition of high-resolution SECM imaging.[26]

All of the above SECM approaches use 25-μm-diameter microelectrodes. The use of such probes can render kinetics constant extraction difficult at short tip-to-substrate distances, given their large overall dimensions (75−250 μm diameters) that can trap and/or regenerate diffusing species from the catalyst layer. Herein, we propose that the use of nanoelectrodes in an SG-TC SECM would be advantageous when studying self-assembled catalysts on gold because they do not significantly disturb the diffusion layer of the substrate and the feedback between the tip and substrate can be neglected. As illustrated in the Theoretical Study section, these two advantages are in fact required if one would like to easily extract catalyst kinetics on the basis of SECM line scans performed at close tip-to-substrate distances.

In the present study, SG-TC measurements have been performed with nanoelectrodes. For long electrolysis times, the concentration profiles are stationary and similar to that of a Nernst layer, even in the absence of forced convection, as extensively discussed in the literature.[27,28] As illustrated in the Theoretical Study section, this study enables some kinetic quantification across the surface of a catalyst. The proposed method thus allows differentiation between catalyst regions homogeneously modified from mixed response regions where both the catalyst and underlying gold contribute to the measured signal.

Experimental Section

Materials and Reagents. Electrochemical measurements were performed in nanopure water solutions purified with a Millipore Milli-Q Biocel Ultrapure water system (Fisher, Ottawa, ON), ferrocene methanol ($FcCH_2OH$) (97%, Aldrich, Canada), and potassium chloride (KCl) or 0.5 M sulfuric acid (H_2SO_4) (Fisherbrand, Canada). Electrochemical solutions were oxygenated for 10 min with oxygen (Praxair oxygen, Canada) prior to each measurement, giving a concentration of 1.2 mM at ambient temperature and pressure. 5,10,15,20-Tetraphenyl-21*H*,23*H*-porphine cobalt(II) (Co-TPP) and 4-aminothiophenol 97% (4-ATP) were purchased from Sigma. Electrode fabrication materials used were a 25-μm-diameter Pt wire (purity 99.9%; hard) (Goodfellow), quartz capillaries (*L*, 150 mm; o.d., 1 mm; i.d., 0.3 mm) (Sutter Instrument), electrically conductive silver epoxy (EPO-TEK H20E) (Epoxy Technology Inc., Canada), and standard copper connection wires (diameter < 0.3 mm). Polishing materials (Buehler, Canada) used were abrasive discs (800, 1200 grit), diamond lapping film discs (1, 0.3, 0.05 μm diamond size), and alumina suspensions (1, 0.3, and 0.05 μm particle diameter).

Electrochemical Cell. The substrates used in the approach curve and the SECM image were 2- and 3-mm-diameter gold electrodes and a 3-mm-diameter glassy carbon electrode (Bioanalytical Systems Inc., Canada). The counter electrode was a platinum wire. All potentials were relative to a Ag/AgCl (3 M NaCl) pseudoreference electrode that was calibrated in $FcCH_2OH$.

Apparatus. A laser puller (P-2000, Sutter Instrument Company, Novato, CA) was used to produce the nanoelectrodes. The CVs, SECM images, and approach curves were generated using either a biological ElProScan system (HEKA, Germany)[29] or a 100 nm ELPro Scan system (HEKA, model PG 340).

Nanoelectrode Fabrication. Many laboratories achieved the development of a reproducible procedure for the fabrication of Pt disk nanoelectrodes using laser pullers.[30−36] In our protocol, an additional thinning step was added to better control the resulting RG ratio of the nanoelectrodes.

Quartz capillaries were cleaned with a dilute (10% v/v) nitric acid solution, rinsed with water, and allowed to dry in an oven. The 25-μm-diameter Pt wire was cleaned with acetone, rinsed with deionized water, and connected to a 0.2 mm copper wire with silver epoxy before heat curing. In the first step, the empty quartz capillary is prethinned using a single line program (heat, 600; filament, 3; velocity, 60; delay, 140; pull, 0). The Pt assembly is then inserted into the center of the capillary. Both ends of the

(19) Sánchez-Sánchez, C. M.; Rodríguez-López, J.; Bard, A. J. *Anal. Chem.* **2008**, *80*, 3254–3260.
(20) Horrocks, B. R.; Schmidtke, D.; Heller, A.; Bard, A. J. *Anal. Chem.* **1993**, *65*, 3605–3614.
(21) Wittstock, G.; Strübing, A.; Szargan, R.; Werner, G. *J. Electroanal. Chem.* **1998**, *444*, 61–73.
(22) Wittstock, G. *Anal. Chem.* **1997**, *69*, 5059–5066.
(23) Evans, S. A. G.; Brakha, K.; Billon, M.; Mailley, P.; Denuault, G. *Electrochem. Commun.* **2005**, *7*, 135–140.
(24) Shen, Y.; Trauble, M.; Wittstock, G. *Anal. Chem.* **2008**, *80*, 750–759.
(25) Eckhard, K.; Schuhmann, W. *Electrochim. Acta* **2007**, *53*, 1164–1169.
(26) Fernández, J. L.; Bard, A. J. *Anal. Chem.* **2003**, *75*, 2967–2974.
(27) Amatore, C.; Szunerits, S.; Thouin, L.; Warkocz, J. S. *J. Electroanal. Chem.* **2001**, *500*, 62–70.
(28) Baltes, N.; Thouin, L.; Amatore, C.; Heinze, J. *Angew. Chem., Int. Ed.* **2004**, *43*, 1431–1435.
(29) Cougnon, C.; Bauer-Espindola, K.; Fabre, D. S.; Mauzeroll, J. *Anal. Chem.* **2009**, *81*, 3654–3659.
(30) Pendley, B. D.; Abruna, H. D. *Anal. Chem.* **1990**, *62*, 782–784.
(31) Fish, G.; Bouevitch, O.; Kokotov, S.; Lieberman, K.; Palanker, D.; Turovets, I.; Lewis, A. *Rev. Sci. Instrum.* **1995**, *66*, 3300–3306.
(32) Shao, Y.; Mirkin, M. V.; Fish, G.; Kokotov, S.; Palanker, D.; Lewis, A. *Anal. Chem.* **1997**, *69*, 1627–1634.
(33) Katemann, B. B.; Schuhmann, W. *Electroanalysis* **2002**, *14*, 22–28.
(34) Sun, P.; Mirkin, M. V. *Anal. Chem.* **2006**, *78*, 6526–6534.
(35) Mauzeroll, J.; LeSuer, R. J. In *Handbook of Electrochemistry*; Zosky, C. G., Ed.; Elsevier: Oxford, U.K., 2007; pp 199−211.
(36) Zhang, B.; Galusha, J.; Shiozawa, P. G.; Wang, G.; Bergren, A. J.; Jones, R. M.; White, R. J.; Ervin, E. N.; Cauley, C. C.; White, H. S. *Anal. Chem.* **2007**, *79*, 4778–4787.

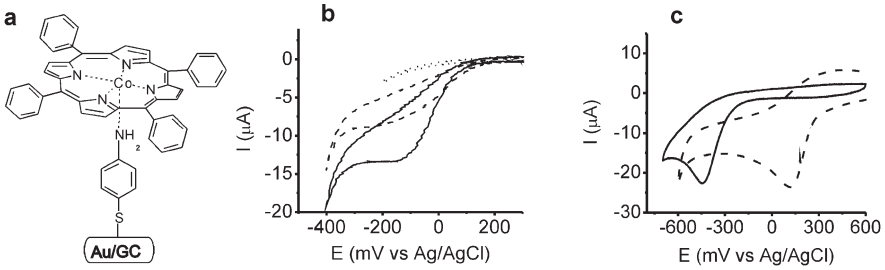

Figure 1. (a) Scheme of 4-ATP-CoTPP deposited on Au and glassy carbon (GC) substrates. (b) Cyclic voltamogramms of bare gold (——), passivated gold with 4-ATP (---), and a catalytically active Au-4-ATP-CoTPP substrate (— —). (c) Cyclic voltamogramms of bare GC (——) and a catalytically active GC-4-ATP-CoTPP substrate (---). The cyclic voltamogramms were recorded in O_2-saturated 0.5 M H_2SO_4 at a scan rate of 100 mV s^{-1}.

capillary are connected to a vacuum pump via flexible silicone tubes and a Y connector. During sealing, weak pulling forces on the glass capillary are avoided using two stoppers that fix the puller bars. Sealing of the Pt wire into the quartz capillary was achieved using a single line program (heat, 540; filament, 5; velocity, 60; delay, 140; pull, 0), repeated for five cycles. A cycle consists of 40 s of heating followed by 20 s of cooling. Following the removal of the stoppers and silicon tubes, the pulling program (heat, 780; filament, 12; velocity, 160; delay, 100; pull, 200) is applied. The resulting microelectrodes were polished with 0.3 and 0.05 μm diamond lapping films. The polishing procedure consists of fixing the microelectrode in the brass cylinder of the rotating disk electrode rotated at 8000 rpm, before the diamond lapping film was moved slowly toward the microelectrodes using a micrometer screw in order to expose the top of the Pt wire.[33]

Metalloporphyrin-Modified Substrates. A gold electrode and a GC electrode (Bioanalytical Systems Inc., Canada) were polished on a microcloth (Buehler, Canada) in combination with 1 and then 0.3 μm alumina slurries (Buehler, Canada). Both electrodes were rinsed with deionized water in the ultrasonic bath for 10 min. The GC electrode was electrochemically oxidized by cycling the potential 15 times between −0.45 and 1.85 V vs Ag/AgCl (3 M NaCl) at 100 mV s^{-1} [37] before modification with the catalyst. In case of the Au electrode, the porphyrin modification was performed after the polishing procedure. The porphyrin modification process consists of immersing the electrodes in a 10 mM ethanol solution of 4-ATP for 2 h, rinsing, and then immersing them in a chloroform solution containing 1 mM CoTPP for 18 h.[12]

SECM Procedures. SECM procedures included nano- and microelectrode characterization using feedback mode and imaging measurements, constant height imaging of metalloporphyrin-modified substrates with 25-μm-diameter Pt microelectrodes, and constant height imaging of metalloporphyrin-modified substrates with nanoelectrodes.

Nanoelectrodes and microelectrodes were characterized using steady-state voltammograms in bulk solution by scanning the potential anodically in the 0 to 600 mV range. The feedback approach curves recorded while approaching carbon and gold substrates were acquired while the nanoelectrode and microelectrode were poised at 400 mV. The approach rate to the substrate surface varied as they were adapted to the microelectrode diameter. Line scans and images were acquired at a scan rate of 95 μm s^{-1} and an applied potential in the 700 to 900 mV range, which oxidizes the H_2O_2 produced by the underlying biased substrate.

Constant height imaging of metalloporphyrin-modified substrates with nanoelectrodes required the prepositioning of the working electrode using the shear force controller of the instrument.[29] The laser-pulled electrodes were connected to a driver and receiver piezoelectric plates, as initially proposed by the Schuhmann group.[38] Following the acquisition of frequency spectra far from the substrate and in close proximity to the substrate, a working resonance frequency, which presents both amplitude and phase sensitivity, is selected. The resonance frequency is then applied at the microelectrode to ascertain the tip-to-substrate distance and preposition the electrode at a tip-to-substrate distance of 6 μm. Constant height images and line scans are then performed.

Results and Discussion

Electrochemical Characterization of the 4-ATP-CoTPP Catalyst Layer. The impact of the applied bias on the local electrocatalytic activity of metalloporphyrin-modified substrates has been studied at different substrates (glassy carbon[10] and gold[16]) that have been produced through different means (chemisorption,[12,39] self-assembly,[16] and electrochemical deposition[40]). The complete self-assembly process produces a stable, highly ordered conducting film, where a cobalt porphyrin (CoTPP) is complexed with 4-aminothiophenol (4-ATP) chemisorbed on a gold substrate.[11] In the case of a glassy carbon (GC) surface, few results were reported for the catalyst[41] and the exact attachment mechanism remains ill-defined. The catalytic activity of the catalyst chemisorbed on both gold and GC electrodes was monitored using cyclic voltammetry in a 0.5 M H_2SO_4 solution saturated with oxygen.

Figure 1a shows the adsorption scheme of CoTPP on a gold substrate and a GC substrate via 4-ATP. On gold, the porphyrin is generally well organized as shown by AFM characterization and reported in the literature[16] (Figure 1 in Supporting Information). It was shown elsewhere[12−14] that thiol molecules could be chemisorbed onto oxidized GC electrodes. Different mechanisms for the adsorption of sulfur on carbon substrates have been suggested; however, these studies are in agreement that sulfur compounds seem to react with defects and surfaces containing an electron-withdrawing element such as nitrogen or oxygen.[12] It was also reported that there is a possibility to obtain a 4-ATP monolayer at the GC electrode after 45 min depending on the GC surface treatment.[12] The CoTPP molecule (19 Å) is approximately 4 times larger than 4-ATP (4.3 Å), so at least four molecules of 4-ATP should be covered by one CoTPP. However, the GC surface chemistry is ill-defined and depends on the presence of carbon−oxygen functional groups at the graphitic edge plane, which might not allow full monolayer coverage of the GC electrode.

(37) Barbero, C.; Silber, J. J.; Sereno, L. *J. Electroanal. Chem.* **1988**, *248*, 321–340.
(38) Ballesteros Katemann, B.; Schulte, A.; Schuhmann, W. *Electroanalysis* **2004**, *16*, 60–65.
(39) Yoshimoto, S.; Inukai, J.; Tada, A.; Abe, T.; Morimoto, T.; Osuka, A.; Furuta, H.; Itaya, K. *J. Phys. Chem. B* **2004**, *108*, 1948–1954.
(40) Karolien, De W.; Philippe, W.; Eduard, T. *Electroanalysis* **2005**, *17*, 263–268.
(41) Ramìrez, G.; Goya, M. C.; Mendoza, L.; Matsuhiro, B.; Isaacs, M.; Chen, Y. Y.; Arévalo, M.; Henrique, J.; Cheuquepàn, W.; Aguirre, M. J. *J. Coord. Chem.* **2009**, *62*, 2782–2791.

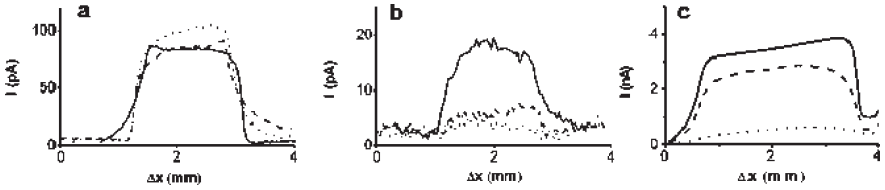

Figure 2. Line scans of bare gold (---), passivated gold with 4-ATP (— —), and a catalytically active 4-ATP-CoTPP substrate (——) recorded at (a) −200 and (b) 100 mV. (c) Line scans of a catalytically active GC-4-ATP-CoTPP substrate recorded at 100 (——), 200 (— —), and 300 mV (---). The line scans were recorded with a 25 μm microelectrode having an *RG* of 10 in O_2-saturated 0.5 M H_2SO_4. The potential applied at the microelectrode was 700 mV. The scan rate was 95 μm s^{-1}, and the tip-to-substrate distance was 30 μm.

The cyclic voltamograms at macroelectrodes (Figure 1b) show the electrochemical behavior of O_2 reduction on bare gold passivated with 4-ATP and a catalytically active 4-ATP-CoTPP substrate. On bare gold, a broad reductive current peak centered at around −100 mV is assigned to O_2 reduction.[42] The peak is not observed in the monolayer-covered gold sample because 4-ATP blocks the ORR. This is consistent with STM data that show that 4-ATP forms dense overlayers on gold.[15] Upon CoTPP complexation to the 4-ATP monolayer, the peak associated with the O_2 reduction is recovered, indicating the catalytic effect of the 4-ATP-CoTPP layer. The obtained shift in the diffusion plateau for bare and catalytically active 4-ATP-CoTPP gold substrates is attributed to differences in oxygen concentration.

Figure 1c shows CVs of a bare GC electrode and that modified with 4-ATP-CoTPP in a 0.5 M H_2SO_4 solution saturated with oxygen. The unmodified GC shows an obvious peak near −450 mV characteristic of O_2 reduction. When the GC electrode is chemically modified with 4-ATP-CoTPP, O_2 reduction occurs at a more cathodic potential, 150 mV, and H_2O_2 is predominantly produced. The mechanisms of the catalytic effect of the CoTPP-GC electrode is well-known in the literature.[16−18]

As such, macroelectrode cyclic voltametry experiments give global information on the electrocatalytic activity of the substrate. Therefore, the homogeneity of the catalyst reactivity on a substrate cannot be easily identified. A local kinetics characterization through scanning electrochemical microscopy measurements has thus been performed.

SECM Measurements of the 4-ATP-CoTPP Catalyst Layer. The substrate's response toward ORR was studied by SG-TC SECM using a classical 25-μm-diameter microelectrode, having an *RG* of 10, in a 0.5 M H_2SO_4 solution saturated with O_2. Because the studied substrate did not present significant topographical features or tilt, constant height measurements were performed. During SECM measurements, a potential of 700 mV was applied at the tip in order to oxidize the peroxide produced on the underlying substrate, which is biased at different potentials. Following a prepositioning of the microelectrode at a tip-to-substrate distance of 30 μm, the microelectrode was moved in a plane parallel to the substrate at a scan rate of 95 μm s^{-1}.

In Figure 2a,b, from left to right, one can see the SECM images of bare gold, passivated gold with 4-ATP, and catalytically active 4-ATP-CoTPP electrodes recorded at −200 and 100 mV applied substrate potentials. The anodic current increase observed when the microelectrode is scanned over the bare gold electrode (Figure 2a) confirms the O_2 reduction on bare gold and subsequent H_2O_2 production and collection at the nearby microelectrode. The 4-ATP-CoTPP-modified electrode shows a positive current indicative of H_2O_2 generation from the ORR at the substrate. For the 25-μm-diameter microelectrode, a homogeneous current is recorded over the entire catalyst layer indicating that 4-ATP-CoTPP is assembled uniformly on the entire electrode active area. The chemical stability of the 4-ATP-CoTPP catalyst layer is maintained up to −500 mV applied substrate potential as expected for strong affinity underlayers involving gold and sulfur interactions. Beyond −500 mV, desorption of the catalyst layer can be visualized in SECM images (Figure 3 in Supporting Information) through the presence of large irregularities on the current plateau using a 32-nm-diameter microelectrode. The SECM images are in line with the CV behavior of similar 4-ATP-porphyrin catalyst layers at anodic potentials, which was attributed to desorption of the catalyst.[43]

In Figure 2c, a catalytically active 4ATP-CoTPP GC electrode was biased at different potentials. At a 300 mV applied potential, a negligible H_2O_2 quantity is oxidized at the UME, thus showing a weak catalytic effect. At more cathodic substrate potentials, such as 200 and 100 mV, a higher oxidation current was measured at the UME. The increase in current is obtained over the entire GC electrode diameter (3 mm) and suggests a homogeneous distribution of the catalyst. Small current variations between the two extremities of the GC electrode can be explained by the substrate tilt.

The use of nanometer-scale electrodes (radius between 20 nm and 1 μm) is advantageous when studying self-assembled catalysts on gold because they do not significantly disturb the diffusion layer of the substrate, the feedback between the tip and the substrate is neglected, and they allow high lateral resolution imaging. This is important when studying metalloporphyrin-modified gold substrates because the underlying gold substrate can generate an additional interfering H_2O_2 flux. A method for developing Pt disk nanoelectrodes and microelectrodes using laser pullers was performed. The technical details and characterization results will be published elsewhere.

These laser-pulled nanoelectrodes were used to study the homogeneity of the porphyrin catalyst and to extract kinetic parameters. A probe diameter of about 460 nm was used to scan the electrocatalytic activity of the substrate coating, which minimizes physical perturbations related to the presence of the probe.

Electrochemical Characterization of the 4-ATP-CoTPP Catalyst Layer Using a Nanoelectrode. The laser-pulled microelectrodes were used to acquire SECM image and line scans of Au-4-ATP-CoTPP catalysts in Figure 3. Positioning of the electrode tip at a known distance above the substrate has been achieved by shear-force constant distance SECM (Figure 4 in Supporting Information). Consistent with the results obtained at 25-μm-diameter microelectrodes, the extent of ORR increases when the applied substrate potential decreases. The largest current recorded is inferior to 2 pA and was obtained at a substrate potential of 0 mV.

Despite the symmetric substrate and tip geometries, an inhomogeneous increase in current is obtained on the left-hand-side of

(42) Genshaw, M. A.; Damjanovic, A.; Bockris, J. O. M. *J. Electroanal. Chem.* **1967**, *15*, 163–172.

(43) Xiaoquan, L.; Limin, Z.; Minrui, L.; Xiaoqiang, W.; Yan, Z.; Xiuhui, L.; Guofang, Z. *ChemPhysChem* **2006**, *7*, 854–862.

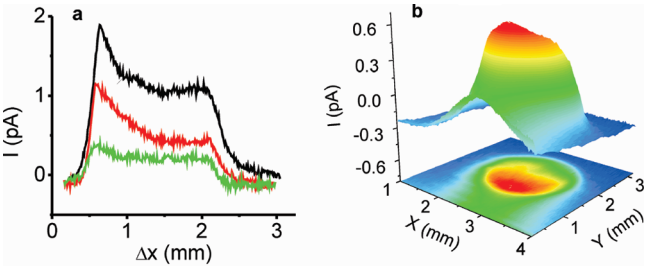

Figure 3. (a) Lines scan of the Au-4-ATP-CoTPP substrate recorded at 0 (black line), 100 (red line), and 200 (green line). (b) SECM image of a Au-4-ATP-CoTPP substrate recorded at a potential of 0 mV. A 460-nm-diameter microelectrode with an *RG* of 8 was biased at 900 mV and positioned 6 μm from the substrate. The measurements were recorded in O_2-saturated 0.5 M H_2SO_4 at a scan rate of 90 μm s^{-1}.

the line scans. Given the overall 2 μm diameter of the scanned tip, convection effects are not dominant. The asymmetry of the electrochemical images observed under substrate generation tip collection conditions is related to differences in the diffusion field of the scanning tip. Because the substrate is biased at a fixed potential and the electrocatalytic layer is on the order of a monolayer of porphyrin molecules, we postulate that the observed asymmetry results from inhomogeneity in the adsorbed porphyrin layer resulting in the combined current contribution of gold and porphyrin at the applied substrate potentials. The applied substrate potential dependence on the presence of the asymmetric current collection also implies that to uniquely isolate the contribution of the porphyrin electrocatalyst toward ORR, measurements should be performed at an applied substrate potential of 200 mV.

The effect of the tip scan rate on feedback current measurements was reported. The substrates used in these studies were unbiased carbon fiber[44] and platinum substrates having dimensions on the order or smaller than that of the scanned tip.[45] It is unlikely that the present observed asymmetry is related to the scan rate because with decreasing cathodic substrate potential the extent of ORR decreases, leading to decreases in the peroxide concentration profile generated at the substrate. Also, had the scan rate been the dominant effect, the dependence on substrate potential would not have been as important.

To probe the homogeneity of the electrocatalyst on a large scale, an SECM image of the 2 mm modified gold-biased substrate at 0 mV was acquired using a 460-nm-diameter microelectrode with a *RG* of 8 under the same conditions as the lines scan (Figure 3b). As expected, the Au electrode was modified with 4-ATP-CoTPP and then displayed activity toward ORR. The asymmetric shape of the acquired image is in accordance with line scan results.

Theoretical Study

SG-TC SECM measurements performed at a long electrolysis time produce steady-state concentration profiles similar to that of a Nernst layer, even in the absence of forced convection.[27,28] This enables the extraction of kinetics constants across the surface of a catalyst. In the present model, special care is given to the influence of the probe used to perform measurements. The model used to describe the processes involved is mainly taken from literature. Specifically, the substrate behavior is modeled according to the work of Shen et al.,[24] and the transport in solution is modeled according to the work of Amatore et al.[27] and Baltes et al.[28]

Concentrations of H_2O_2 and O_2 are noted as $[O_2]$ and $[H_2O_2]$. At the substrate with radius r_s, a complex process occurs whereby O_2 is consumed and H_2O_2 is produced. The main reaction pathways are

reduction of O_2 into H_2O_2

$$O_2 + 2H^+ + 2e^- \xrightarrow{k_1} H_2O_2 \quad (1)$$

reduction of O_2 into H_2O

$$O_2 + 4H^+ + 4e^- \xrightarrow{k_2} 2H_2O \quad (2)$$

reduction of H_2O_2 into H_2O

$$H_2O_2 + 2H^+ + 2e^- \xrightarrow{k_3} 2H_2O \quad (3)$$

Such processes consisting of several elementary steps are assumed to follow first-order kinetics toward the electroactive reactant concentration.[24] The effective rate constants, k_i, provides general information on the reaction paths.

In the absence of the macroscopic movement of the solution, the transport of O_2 and H_2O_2 is dominated by hydrodynamic conditions where the complex transport of solutes to the electrode surface area involves both diffusion and convection, even if the solution is macroscopically still.[27,28] This comes from microscopic movements of the solution and has been called spontaneous convection. According to the work from Amatore et al.[27,28] and Baltes et al.,[29] in such a case it is possible to obtain a stationary concentration profile. In contrast to the transient study performed by Shen et al,[24] the present model, consistent with the above SECM experiments, will then involve steady-state conditions. The breadth of the kinetic studies performed with the steady-state approach is not as far reaching as the original transient method. However, it readily allows one to extract catalyst kinetics constants at different tip positions during SECM line scans, evaluate the homogeneity of the surface modification, and optimize the applied substrate potential for a given catalyst layer.

According to previously cited work,[28] the distance where concentration gradients occur (noted l_D) has a value of around 230 μm, which is much smaller than the substrate size (millimeter range). In such a case, in the absence of an SECM probe, the diffusion is planar and 1D reasoning is possible to evaluate the concentration profiles. In addition, according to the same work, the obtained concentration profile is linear over 60% of the region where the diffusion occurs, and the Nernst layer model can then be used to evaluate the concentration variation in this region.

These hypotheses lead to the following conditions on flux densities of O_2 and H_2O_2 at the substrate:

$$(k_1 + k_2)[O_2]_{sub} = D_{O_2}\frac{[O_2]_{sol} - [O_2]_{sub}}{l_D} \quad (4)$$

and

$$k_1[O_2]_{sub} - k_3[H_2O_2]_{sub} = D_{H_2O_2}\frac{[H_2O_2]_{sub}}{l_D} \quad (5)$$

This, in addition to the hypothesis of linear variation of concentration with distance, z, from the substrate, leads to the following expression of concentration:

$$[H_2O_2]_z = \left(1 - \frac{z}{l_D}\right)\frac{k_1}{\frac{D_{H_2O_2}}{l_D} + k_3}\frac{\frac{D_{O_2}}{l_D}}{k_1 + k_2 + \frac{D_{O_2}}{l_D}}[O_2]_{sol} \quad (6)$$

(44) Xiong, H.; Guo, J.; Amemiya, S. *Anal. Chem.* **2007**, *79*, 2735–2744.
(45) Macpherson, J. V.; Slevin, C. J.; Unwin, P. R. *J. Chem. Soc., Faraday Trans.* **1996**, *92*, 3799–3805.

This expression is assumed to be valid for $z < 0.6l_D$.[28] The following section details how this concentration can be linked to the experimentally accessible tip current. The effect of the probe movement has been neglected because it is assumed that the convection induced by the movement of the tip is not influencing the measurement.

Measurements with Small Probes. If the probe used to evaluate the concentration is small enough, then it does not disturb the concentration profiles so that it is possible to establish a quantitative relation between the concentration obtained without the tip and the current measured at the same position:

$$[H_2O_2]_{z=z_{tip}} = \frac{i_T}{8FD_{H_2O_2}a\beta(RG)} \quad (7)$$

$\beta(RG)$ is a correction factor that takes a value of 1.02 for $RG = 10$ and 1.1 for $RG = 2$. Various analytical approximations of this factor are available in the literature.[46] i_T is the measured current when the tip is biased at oxidative potentials.

This leads to the following relationship between measurable quantities and unknowns:

$$\left(1-\frac{z}{l_D}\right)\frac{8FD_{H_2O_2}a\beta(RG)[O_2]_{sol}}{i_T} = \frac{\left(\frac{D_{H_2O_2}}{l_D}+k_3\right)\left(k_1+k_2+\frac{D_{O_2}}{l_D}\right)}{k_1\frac{D_{O_2}}{l_D}} \quad (8)$$

Measurements with Large Probes. With large probes, the link between the measured current and the concentration at the same position in the absence of a probe is not as simple as that obtained in the case of small probes (eq 7). To quantify this, numerical 2D steady-state simulations have been performed that explicitly take into account the presence of the probe. During the numerical simulations, special care has been given to meshing, especially at conductive parts of the microelectrode. Routine accuracy verifications of the numerical simulations lead to negligible uncertainty in the numerical simulations, in comparison to experimental uncertainty. Focusing on the previously detailed experimental situation, all numerical simulations have been performed with the same geometrical parameters as those used to obtain Figure 3: $a = 12.5\,\mu$m, $RG = 10$, and $z_{tip} = 30\,\mu$m. Other parameters are taken from the literature: $l_D = 230\,\mu$m, $D_{O_2} = 2.0 \times 10^{-5}$ cm^2/s, $D_{H_2O_2} = 1.6 \times 10^{-5}$ cm^2/s, and $[O_2]_{sol} = 0.27$ mmol/L. Figure 4 shows the deduced concentration from current measurements by directly using the previously presented equation (eq 7) that is valid for small probes, as a function of kinetics constant k_1 for different values of k_3 (k_2 is taken to be equal to 0). In eq 7, iT has been evaluated through numerical simulations as detailed above. In addition, for each case, the concentration that would be obtained at the same position in the absence of the probe (according to eq 6) is presented. The kinetics constant axis is on the logarithmic scale in order to cover the whole range of kinetic behavior: small kinetics constants values, where the substrate can be considered to be nonreactive and the produced quantity of H_2O_2 is small, and large kinetics constants, where the production of H_2O_2 is limited by the transport of matter (concentration of O_2 at the substrate is then 0).

In all cases, there is a significant difference between curves. Moreover, as shown for the curves obtained for $k_3 = 0.1$ m/s, in the case of an alternating pathway consuming H_2O_2, the relation between the measured signal and the expected one can be complicated. The difference between the two is due to two main effects: first, the consumption of H_2O_2 at the probe produces O_2. This produced O_2 is an additional contributing flux to that coming from bulk and thus increases the H_2O_2 produced by the substrate. This is the feedback effect. In addition to this, one has to be aware of the fact that the presence of the probe, including the surrounding glass thickness, hinders diffusion and may also lead to an inappropriate evaluation of current. As such, the various processes occurring at substrate lead to the introduction of a correction factor (corr) that has to be considered when data are obtained with micrometer-scale probes:

$$\frac{i_T}{8FD_{H_2O_2}r_T\beta(RG)} = \mathrm{corr}[H_2O_2]_{z=z_{tip}} \quad (9)$$

In Figure 4, this correction factor would correspond to the ratio of the two curves in each situation, and eq 8 is subsequently changed. The correction factor depends not only on geometric parameters (l_D, a, RG, and z_{tip}) but also on kinetics constants, as illustrated in Figure 4. This could offer the possibility of multiple kinetics constant characterization because the measured signal is likely to depend on more than one kinetic parameter combinations, as was the case with nanoelectrodes. However, such a study would require extensive numerical simulation work and is beyond the scope of this article.

Interpretation of Experimental Results: Influence of Substrate Potential on Kinetics Constants. The developed model can be used to interpret the SECM line scans obtained with nanoelectrodes probing an underlying catalyst layer. In this first attempt and because of the complexity of the system under consideration, where many pathways are possible, we have focused our attention on the first reaction path, which leads to the partial reduction of O_2 to H_2O_2 and is thus expected to be most favored at cathodic substrate potentials. To extract k_1 from nanoelectrode measurements, a simplification and reorganization of eq 8 leads to

$$k_1 = \frac{D_{O_2}}{l_D\left(1-\frac{z}{l_D}\right)\frac{8FD_{O_2}r_T\beta(RG)[O_2]_{sol}}{i_T} - l_D} \quad (10)$$

From the measurements presented in Figure 5a, it is possible to evaluate k_1 for each microprobe position and each substrate potential. Because of the presence of reactivity heterogeneity, results for two positions over the substrate have been considered: one at the border from the substrate where heterogeneity is observed ($\Delta x = 0.6$ mm) and one far from this heterogeneity ($\Delta x = 1.7$ mm). This is presented in Figure 5a (on the logarithmic scale for the kinetics constant axis). From this Figure, it appears that only the region with the heterogeneity does not follow linear behavior. Taking into account experimental uncertainties in parameters such as z_{tip} or $[O_2]_{sol}$ does not significantly change this linear behavior. This makes observed linearity reliable, even if only three substrate potentials have been used. From this, it appears that the simplest model (only one pathway and a simple exponential variation of the kinetics constant with substrate potential) may lead to satisfying agreement with experiments over the main part of the tip. The extracted kinetics values are $\alpha_1 = 0.1$ and $k^0{}_1 = 1.4 \times 10^{-7}$ m/s (corresponding to a constant for $E_s = 0$ V vs reference). To the best of our knowledge, this is the first evaluation of kinetics parameters with self-assembled 4ATP-CoTPP on gold.

In the case of a large tip, as previously illustrated, the presence of the probe disturbs the concentration profile. Thus, a correction

(46) Lefrou, C.; Cornut, R. *ChemPhysChem* **2010**, *11*, 547–556.

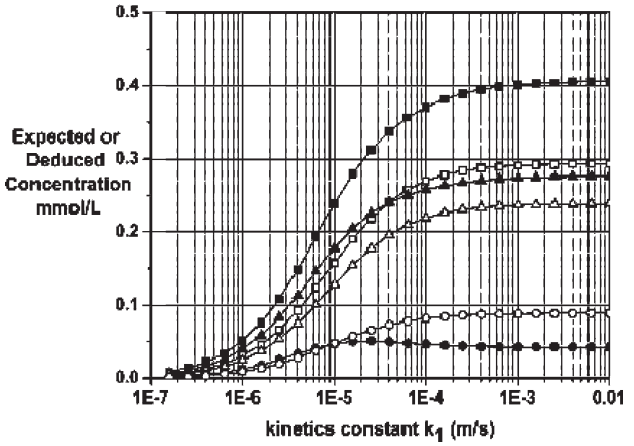

Figure 4. Expected concentration in the absence of a probe (open symbols) according to eq 6 or deduced from current measurement concentrations using eq 7 using solid symbols (see text for more details). as a function of kinetics constant k_1 (m/s): (■, □) k_3 = 0 m/s, (▲, △) k_3 = 0.01 m/s, and (●, ○) k_3 = 0.1 m/s. Other conditions: probe radius = 12.5 μm, RG = 10, z_{tip} = 30 μm, l_D = 230 μm, D_{O_2} = 2.0 × 10^{-5}cm^2/s, $D_{H_2O_2}$ = 1.6 × 10^{-5} cm^2/s, and $[O_2]_{sol}$ = 0.27 mmol/L.

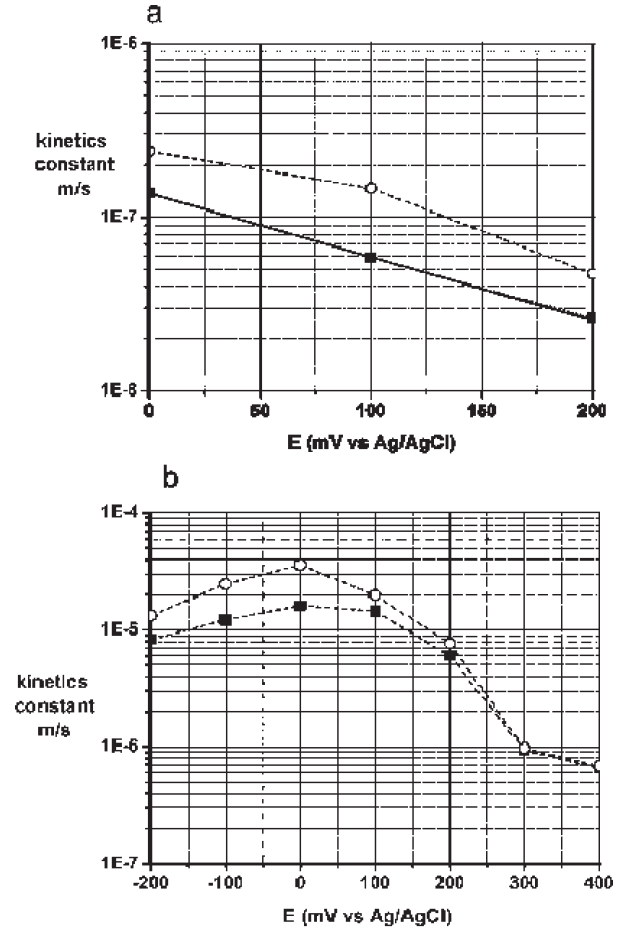

Figure 5. Extracted kinetics constants as a function of substrate potential (a) from measurements presented in part a using eq 10 and (b) from measurements in Figure 3c using eq 11. For both, the extracted kinetics near the border of the substrate (empty circles) and at the center of the substrate (filled squares) are presented.

factor has to be considered between the measured current and the obtained concentration without the tip. This makes data interpretation more difficult because the extraction of the kinetics constant for each substrate potential requires numerical adjustments in addition to numerical simulations:

$$\frac{D_{H_2O_2}\left(k_1+\frac{D_{O_2}}{l_D}\right)}{k_1\mathrm{corr}(k_1)D_{O_2}} = \left(1-\frac{z}{l_D}\right)\frac{8FD_{H_2O_2}r_T\beta(RG)[O_2]_{sol}}{i_T} \quad (11)$$

The extraction procedure leading to k_1 from this equation has been performed, and Figure 5b presents the obtained kinetics constants as a function of substrate potential. It shows that even far from potentials where further reduction of H_2O_2 into H_2O is likely to occur there is no linear behavior that is observed. The lack of linearity has two possible sources: either k_1 does not have an exponential dependence on the substrate potential or other pathways occur even at high potentials. In this later case, the extraction of kinetics parameters is complicated and cannot be done only with the line scans presented in the Experimental Section of this article.

Conclusions

The detection of H_2O_2 generated at electrocatalytic surfaces during the ORR is important in evaluating the potential performance of materials in fuel cells and air batteries. As such, the SG-TC mode of the SECM is a useful alternative to the more classical method of a rotating ring disk electrode. In characterizing the modification of thiol-porphyrin films on gold electrodes using the SG-TC mode of the SECM, we show the blocking effect of self-assembled monolayers and the electrocatalytic activity of the 4-ATP-CoTPP catalyst layer. Consistent results were obtained from conventional cyclic voltammetry and from SECM recorded at 25-μm-diameter electrodes and disk laser-pulled nanoelectrodes. The use of geometrically well-defined Pt nanoelectrodes is advantageous because it limits the physical disturbance of the generated concentration profiles and probes the homogeneity of the assembled catalyst. It also allows the identification of the optimal applied substrate potential, which uniquely isolates the electrocatalytic contribution of the metallophorphyrin. As illustrated in this article, a quantitative interpretation of experiments with micrometric tips is not as straightforward as that with nanometric tips, which do not necessarily require numerical simulations for interpretation. On the basis of this study, we will extend our research to a set of substrates and porphyrin self-assembled systems,which will enable us to evaluate the effect of porphyrin orientation and the extent of substrate interaction on the overall ORR activity and H_2O_2 generation.

Acknowledgment. We acknowledge the Natural Sciences and Engineering Research Council of Canada (NSERC) and the Canadian Foundation for Innovation (CFI) for their financial support. Dr. Matthias Geissler of the Industrial Materials Institute-National Research Council of Canada is graciously acknowledged for his gift of gold disk patterned arrays deposited on silicon. Dr. Jack Belgum of the Sutter Instrument Company is acknowledged for useful discussions. Dr. A. Badia and M.Sc. E. Dionne are acknowledged for their AFM contributions.

Supporting Information Available: AFM images of a bare Au substrate and a catalytically active Au-4-ATP-CoTPP substrate. SECM image of a catalyst with a 25-μm-diameter electrode. Thiol desorption SECM image. Distance calibration of the phase and amplitude rectification prior to constant-height microscopy. Axis orientations and geometric parameters of the modeled system. This material is available free of charge via the Internet at http://pubs.acs.org.